Geochemical Journal Vol. 16, pp. 199 to 212, 1982

Effect of diagenetically remobilized metals on regional difference in manganese nodules

SHIZUO TSUNOGAI, KEITA NAKANISHI and MASATOSHI YAMADA

Department of Chemistry, Graduate School of Fisheries,
Hokkaido University, Hakodate 041, Japan

(Received February 10, 1982: Accepted August 25, 1982)

Pelagic manganese nodules were sampled at two sites. One was in the subtropical Pacific where the biological productivity in the surface water was low and Mn did not migrate in the surface sediment. The other was in the equatorial Pacific where manganese oxide in the sediment was reduced by organic material and dissolved Mn was lost from the sediment to the bottom water. It has been demonstrated that the difference in the sedimentary environment is reflected in manganese nodules. The bottom surface of the equatorial nodules contained larger amounts of transition metals soluble in weak acids than other sides in contact with sea water and the acid soluble metals decreased with depth from the bottom surface. On the bottom side of the equatorial nodule the oxide fractions of Cu and Ni increased with depth, indicating the trapping of metals which diffused through the pore waters of sediments and nodules. The bottom surface of the larger subtropical noudles contained much smaller amounts of ^{230}Th than other surfaces, but the growth rate obtained from the depth profile of ^{230}Th was similar to those of the other surfaces. The smaller subtropical nodules contained a normal amount of ^{230}Th at the bottom surface. The concentration of ^{232}Th decreased with depth at each surface, that is, with time, except for the bottom surface of the larger subtropical nodules, in which ^{232}Th concentration is similar to that in the interior of nodules. These observations apparently lead to the conclusion that the bottom surface of the larger subtropical nodules are not growing at present, but the following possibility can not be excluded. The bottom surface is now growing with Th supplied chiefly from weathering debris rather than authigenic particles in sea water.

INTRODUCTION

The origin of ferro-manganese nodules or crusts in the ocean is still an unsolved problem actively studied at present (e.g. project MANOP in U.S.A. as stated by MOORE *et al.*, 1981). Many authors have considered the effect of volcanic or hydrothermal activities to be important in the genesis of nodules as reviewed by CRONAN (1976), HARADA (1977) and others. We (TSUNOGAI *et al.*, 1979; TSUNOGAI and KUSAKABE, 1982), however, have concluded that the amount of manganese entering the ocean from the continents is almost balanced by its removal into sediments because most Mn in oxidizing surface sediments is diagenetically dissolved when the sediments become reducing in the subsurface layer, and the Mn migrates to the sediment-water interface where it is re-oxidized and precipitated. We have further stated that the mobility of Mn in the sediments is highly dependent on organic carbon (a reducing agent) content of sediments, that is on the biological productivity in the overlying surface water as far as the water depth is nearly the same.

If manganese nodules are formed primarily from the diagenetically remobilized Mn in sediments, the nodules will be somewhat different in concentration and accretion rates of some metastable components depending on place where they have grown. Even individual nodules will differ from part to part reflecting variability in the period between the supply of manganous ions to the oxygenated water and the deposition of manganese oxide on the surface of nodules. We have studied nodules collected at two sites which differ in biological productivity of surface

water using chemical and radiochemical techniques. The results indicate the mechanism of formation of nodules to be the diagenetic remobilization and precipitation of Mn and other metals as proposed by TSUNOGAI and KUSAKABE (1982).

MATERIALS AND METHODS

The nodules used in this study were collected from two cruises in the western North Pacific by box coring (KH-79-4) and dredging (GH-78-1). The site of KH-79-4 samples (20°01'N, 158°33'E; 5,560m water depth) was a subtropical region where biological productivity in surface water was extremely low and bottom sediments consisted of red clay. The GH-78-1 samples were collected in a tropical region (8°00'N, 176°57'E; 5,200m water depth) where surface water was rather productive owing to the equatorial upwelling. The sediment consists of siliceous ooze, containing considerably large amount of biogenic silica.

The nodules were ellipsoidal in shape and had lines of apsides of 5 to 10cm. Layers of nodule material were scraped off from the top, sides and bottom of the nodules with a dental drill. The thickness of each scraped layer was 0.1 to 1.0mm. This was estimated from the area scraped and the weight of sample by assuming the density of nodules is 2g/cm^3 (KU and BROECKER, 1969). The original orientation of nodules was relatively easily recognized even in the dredge samples because the top surface was rather smooth while the bottom surface which contained clay particles from sediments was coarse.

The chemical separation technique used was principally the same as that of TSUNOGAI *et al.* (1979) for sediments. We used a 6% acetic acid solution instead of 25% warm solution because the stronger acid solution gradually decomposed the oxide phase of samples. We obtained satisfactory results with 6% acetic acid as shown in Fig. 1, in that the concentrations of metals dissolved at a room temperature did not increase with time. The chemical separation technique used in this study is as follows.

First, 10ml of distilled water is added to about 10mg of a nodule sample dried at 110°C in a glass tube, which is shaken for 15min. at a room temperature and allowed to stand over night. After centrifuging at 3,000rpm, the supernatant solution is discarded. This procedure removes sea salts. This is necessary to avoid a reaction of manganese oxide with chloride in acid solution. Second, 10ml of 6% (1M) acetic acid solution is added to the sample remaining in the glass tube. The solution is shaken for 15min. After 5 hours, supernatant (fraction A) is separated by centrifugation. The leaching procedure is then repeated with 10ml of a mixture 6% (1M) acetic acid and 1M hydroxylamine hydrochloride (a reducing agent). The leachant is designated as fraction B. Finally the dried solid residue is put into a sealed teflon vessel with 300μl of concentrated nitric acid, 300μl of concentrated perchloric

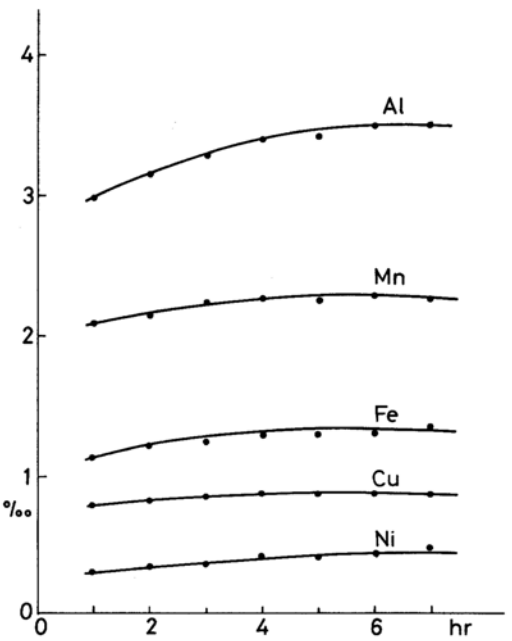

Fig. 1. Variations of the weak acid soluble fractions of various metals in nodule samples with time of reaction. About 10mg of a nodule sample in 10ml of 1M acetic acid solution was allowed to stand for a given time with occasional stirring at a room temperature.

acid and 100μl of concentrated hydrofluoric acid, and heated overnight at 150°C (NORIKI *et al.*, 1980). This solution is called fraction C which is composed mainly of aluminosilicate material.

Acetylene-air flame atomic absorption spectrophotometry was used for the determination of Fe, Mn, Co and Ni. Aluminum was determined by acetylene-nitrous oxide flame atomic absorption spectrophotometry. Flameless atomic absorption spectrophotometry was used to determine Co, Ni and Cu. Dissolved silicate was determined by the standard colorimetric method of molybdenum yellow by adding boric acid as a masking agent for fluoride.

Thorium isotopes were radiochemically analyzed by digesting about 100mg of a nodule sample without application of the successive separation treatment. Thorium in the solution was purified with an anion exchange resin and chemical separation techniques, and electrodeposited onto a silver disc from a hydrochloric acid and ethanol solution. The α activities of ^{228}Th, ^{230}Th and ^{232}Th were counted with a spectrometer equipped with a surface barrier silicon detector. The chemical yield was determined by counting the β activity of ^{234}Th added before the analysis. The yield ranged from 80 to 95%.

Mineralogical examination was made by N. TAKEMATSU using an X-ray diffraction method.

RESULTS AND DISCUSSION

Depth distributions of various forms of metals

The results obtained with the successive chemical separation technique for metals and silica are shown in Table 1. There is a large difference but a definite tendency in the values of the GH-78-1 (the equatorial Pacific) samples. To show the tendency clearer we have calculated the ratio of the weak acid soluble fraction (A) to the total soluble fraction (A+B) as given in Table 2, and plotted in Fig. 2 for Mn and Fig. 3 for Ni.

The most remarkable feature in Fig. 2 is that the bottom surface of the equatorial nodule (GH-78-1) is extremely enriched in weak acid soluble Mn. Further, the enrichment decreases with the distance from the surface. Conversely the bottom surface of the subtropical nodule (KH-79-4) is not enriched in Mn compared with its top surface. The enrichment of weak acid soluble Mn in the surface layer relative to deeper layers is present in all samples. In the equatorial Pacific Mn in the sediment is diagenetically remobilized and supplied to the botttom water through pore waters (TSUNOGAI and KUSAKABE, 1982). It is natural to consider that a metastable form of solid Mn is contained more in the bottom surface of the equatorial nodules, which was in contact with the sediment supplying remobilized Mn, than in the other surfaces. This observation, therefore, suggests that manganese nodules contain a metastable form (weak acid soluble) of Mn of diagenetic origin. The metastable Mn is transformed to a more stable form with time. The tendency of the bottom surface of the equatorial nodule to contain more metastable forms of metals than the top surface is also reflected in other constituents, Al, Fe, Ni, Cu and Co (Fig. 3 for Ni and Table 1).

The depth profiles of Co and Fe in nodules are generally similar to that of Mn, but those of Ni and Cu are somewhat different from that of Mn (Table 1). The profile of the acid soluble fraction of Co decreasing with depth (Fig. 4) is quite similar to that of Mn. This indicates that Co may behave similarly to Mn during the formation of manganese nodules. This substantiates the observations of TAKEMATSU (1979) and may be due to the similar ionic radii of Mn^{4+} (0.54A) and Co^{3+} (0.54A) in oxides as discussed by BURNS (1976). In the equatorial sample Co in the oxide fraction (B) is more concentrated in the surface 0.3mm layer than in deeper layers, although this feature is not obvious for Mn. If some minor constituents in the nodules are exchanged during the rearrangement of the crystal structure of ferro-manganese oxide, then Co may be excluded from the oxide as well as Th discussed later.

Alternately, the depth distribution of Cu in the oxide fraction (B) in the GH-78-1 (the equatorial Pacific) sample shows an increase with

Table 1. Concentrations of Mn, Fe, Al, Si, Ni, Cu and Co in the fractions A (weak acid soluble), B (oxide), and C (refractory material) of the sediments.
KH-79-4 (subtropical Pacific) and GH-78-1 (equatorial Pacific)

KH-79-4	Mn				Fe				Al				Si
Depth (mm)	A (ppm)	B (%)	C (ppm)	Σ (%)	A (ppm)	B (%)	C (%)	Σ (%)	A (ppm)	B (ppm)	C (%)	Σ (%)	Σ (%)
Top													
0-0.08	6,040	13.4	803	14.1	8,550	14.0	5.04	19.9	2,470	4,170	1.43	2.09	4.53
0.08-0.16	6,630	15.0	681	15.7	8,870	14.7	4.46	20.0	3,110	4,480	1.66	2.42	5.64
0.16-0.29	5,860	14.8	476	15.4	6,370	14.4	3.68	18.4	2,810	4,360	1.65	2.37	5.25
0.29-0.44	5,690	15.1	406	15.7	6.520	13.9	3.32	17.9	2,960	4,280	1.53	2.25	5.56
0.44-0.57	5,930	17.1	525	17.7	6,290	15.4	4.09	20.1	3,440	5,100	2.09	2.94	5.73
Side													
0-0.29	4,900	16.5	–	–	4,610	9.9	–	–	1,810	3,350	1.44	1.96	5.15
0.29-0.68	5,530	19.3	604	19.9	4,160	11.2	3.09	14.7	2,530	4,880	1.00	1.74	4.56
0.68-1.22	3,850	17.6	1,070	18.1	3,720	12.4	5.98	18.8	2,820	5,630	–	–	4.49
1.22-1.91	3,630	16.7	1,270	17.2	2,120	9.6	9.08	18.9	2,140	6,890	0.784	1.69	4.14
Bottom													
0-0.29	4,510	14.6	958	15.1	3,140	10.5	4.52	15.3	4,800	9,120	2.90	4.29	7.43
0.29-0.54	3,850	14.1	652	14.6	3,790	12.6	4.18	17.2	5,150	9,510	–	–	5.90
0.54-0.72	4,190	15.1	–	–	3,540	11.9	4.16	16.4	5,110	9,800	–	–	7.72
0.72-0.93	3,860	16.6	715	17.0	3,230	12.6	5.07	18.0	4,890	10,240	1.89	3.40	5.52
0.93-1.16	3,560	16.0	601	16.4	3,230	12.6	5.02	17.0	4,630	9,620	1.39	2.82	–

KH-79-4	Ni				Cu				Co			
Depth (mm)	A (ppm)	B (ppm)	C (ppm)	Σ (ppm)	A (ppm)	B (ppm)	C (ppm)	Σ (ppm)	A (ppm)	B (ppm)	C (ppm)	Σ (ppm)
Top												
0-0.08	407	2,500	n.d.	2,900	460	837	n.d.	1,300	84.7	4,090	n.d.	4,170
0.08-0.16	469	2,530	n.d.	3,000	593	794	n.d.	1,390	78.0	4,440	n.d.	4,520
0.16-0.29	470	2,380	n.d.	2,850	573	776	n.d.	1,350	56.7	3,880	n.d.	3,940
0.29-0.44	480	2,390	n.d.	2,870	619	743	n.d.	1,360	52.5	3,770	n.d.	3,820
0.44-0.57	572	2,720	n.d.	3,290	726	852	n.d.	1,580	50.2	3,920	n.d.	3,970
Side												
0-0.29	675	5,780	n.d.	6,460	607	1,770	n.d.	2,380	58.5	4,290	n.d.	4,350
0.29-0.68	826	6,250	n.d.	7,080	656	1,400	n.d.	2,060	64.1	6,000	n.d.	6,060
0.68-1.22	634	5,330	n.d.	5,960	594	1,140	n.d.	1,730	49.2	5,350	n.d.	5,400
1.22-1.91	545	5,780	n.d.	6,330	726	1,700	n.d.	2,430	54.0	5,380	n.d.	5,430
Bottom												
0-0.29	463	3,940	n.d.	4,400	1,090	2,080	n.d.	3,170	43.4	3,660	n.d.	3,700
0.29-0.54	369	3,160	n.d.	3,530	1,060	1,580	n.d.	2,640	35.2	3,760	n.d.	3,800
0.54-0.72	460	4,370	n.d.	4,830	1,180	2,120	n.d.	3,300	32.0	3,450	n.d.	3,480
0.72-0.93	502	4,970	n.d.	5,470	1,320	2,430	n.d.	3,750	29.0	3,710	n.d.	3,740
0.93-1.16	476	4,270	n.d.	4,750	1,320	2,060	n.d.	3,380	30.0	3,850	n.d.	3,880

GH-78-1	Mn				Fe				Al				Si
Depth (mm)	A (ppm)	B (%)	C (ppm)	Σ (%)	A (ppm)	B (%)	C (%)	Σ (%)	A (ppm)	B (ppm)	C (ppm)	Σ (%)	Σ (%)
Top													
0-0.34	3,120	17.5	–	–	7,310	13.8	–	–	3,820	4,090	–	–	2.44
0.34-1.40	1,270	19.4	–	–	3,280	14.2	–	–	3,290	3,720	–	–	2.44
1.40-2.83	1,550	19.8	–	–	3,160	14.1	–	–	3,970	4,140	–	–	2.56
2.83-3.29	2,020	16.3	2,670	16.8	3,160	13.2	2.70	16.2	4,940	5,650	6,860	1.75	3.60
Side													
0-0.16	4,690	17.0	1,790	17.6	8,770	16.2	2.32	19.4	3,090	3,310	5,120	1.15	2.47
0.16-0.32	3,040	19.1	2,530	19.7	7,270	15.8	2.16	18.7	3,330	3,990	4,380	1.17	2.50
0.32-0.50	2,340	17.8	1,530	18.2	5,970	14.9	2.12	17.6	3,200	3,870	5,240	1.23	2.55
0.50-0.73	1,600	18.6	2,360	19.0	4,680	15.1	2.45	18.0	3,300	3,740	4,780	1.18	2.55
0.73-0.98	1,610	18.5	2,040	18.9	3,760	14.3	2.09	16.8	3,760	4,030	4,210	1.20	2.17
Bottom													
0-0.33	8,500	15.8	4,140	17.1	10,200	13.6	1.09	15.7	5,470	5,930	4,540	1.59	2.44
0.33-0.53	–	–	–	–	–	–	–	–	–	–	–	–	–
0.53-0.95	7,450	18.1	2,320	19.0	6,550	15.1	1.25	17.0	5,000	5,060	5,540	1.56	2.24
0.95-1.31	6,440	14.6	2.960	15.5	6,120	11.2	0.955	12.8	–	5,130	3,790	–	2.48
1.31-1.82	4,660	18.7	4,070	19.6	4,630	13.0	1.36	14.8	4,440	5,790	–	–	2.51
Interior 20													8.61

To be cont'd

GH-78-1	Ni				Cu				Co			
Depth (mm)	A (ppm)	B (ppm)	C (ppm)	Σ (ppm)	A (ppm)	B (ppm)	C (ppm)	Σ (ppm)	A (ppm)	B (ppm)	C (ppm)	Σ (ppm)
Top												
0-0.34	792	3,670	n.d.	4,460	1,190	980	n.d.	2,270	–	3,710	n.d.	(3,710)
0.34-1.40	736	4,620	n.d.	5,360	1,260	1,500	n.d.	2,760	–	3,330	n.d.	(3,330)
1.40-2.83	765	5,340	n.d.	6,110	1,650	2,030	n.d.	3,680	–	4,160	n.d.	(4,160)
2.83-3.29	573	3,400	n.d.	3,970	1,530	1,370	n.d.	2,900	–	3,450	n.d.	(3,450)
Side												
0-0.16	646	2,630	n.d.	3,280	921	606	n.d.	1,530	–	4,770	n.d.	(4,770)
0.16-0.32	805	3,350	n.d.	4,160	1,020	750	n.d.	1,770	–	3,910	n.d.	(3,910)
0.32-0.50	713	3,030	n.d.	3,740	1,040	757	n.d.	1,800	–	3,530	n.d.	(3,530)
0.50-0.73	729	3,200	n.d.	3,930	1,120	917	n.d.	2,040	–	3,660	n.d.	(3,660)
0.73-0.98	738	3,780	n.d.	4,520	1,230	973	n.d.	2,200	–	3,400	n.d.	(3,400)
Bottom												
0-0.33	990	2,390	n.d.	3,380	1,740	1,150	n.d.	2,890	93.3	4,400	n.d.	4,490
0.33-0.53	–	–	–	–	–	–	–	–	–	–	–	–
0.53-0.95	980	2,460	n.d.	3,440	1,740	920	n.d.	2,680	55.8	3,590	n.d.	3,650
0.95-1.31	1,100	3,060	n.d.	4,160	1,530	1,090	n.d.	2,620	42.6	3,520	n.d.	3,560
1.31-1.82	1,080	3,870	n.d.	4,950	1,710	1,400	n.d.	3,110	30.6	3,670	n.d.	3,700

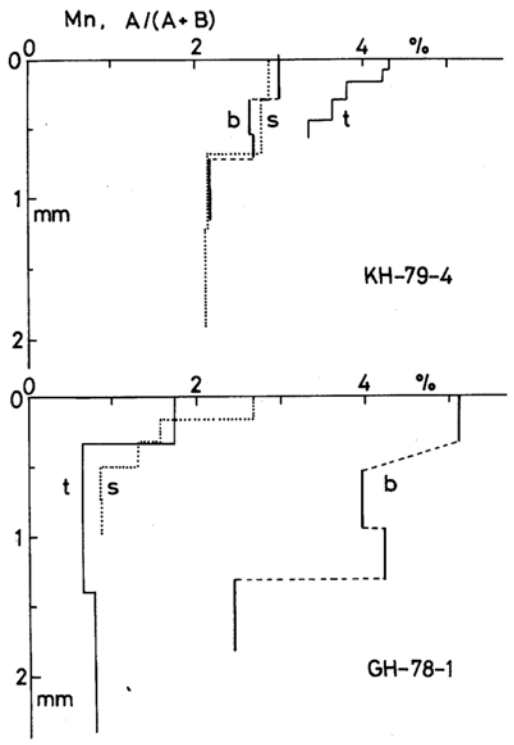

Fig. 2. Depth profiles of ratios of the weak acid soluble fraction (A) to the total acid and reducing agent soluble fraction (A+B) for Mn. The letters in the figure, t, s and b refer to, respectively, the top, side and bottom surfaces of the KH-79-4 and GH-78-1 nodule samples.

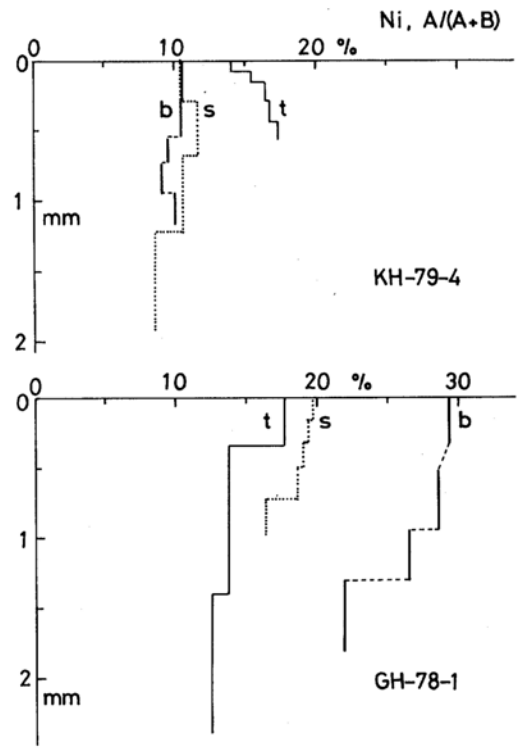

Fig. 3. Depth profiles of ratios of the weak acid soluble fraction (A) to the total acid and reducing agent soluble fraction (A+B) for Ni. The symbols are the same as those in Fig. 2.

Table 2. Concentration ratios of the weak acid soluble fraction (A) to the sum of acid and reducing agent soluble fractions (A+B) for Mn, Fe, Al, Ni, Cu and Co in the nodule samples.

Depth (mm)	Mn (%)	Fe (%)	Al (%)	Ni (%)	Cu (%)	Co (%)
KH-79-4						
Top						
0-0.08	4.31	5.75	37.1	14.0	35.4	2.02
0.08-0.16	4.23	5.69	40.9	15.6	42.7	1.72
0.16-0.29	3.80	4.32	39.1	16.4	42.4	1.44
0.29-0.44	3.63	4.48	40.8	16.7	45.4	1.37
0.44-0.57	3.35	3.92	40.2	17.3	46.0	1.26
Side						
0-0.29	2.88	4.44	35.0	10.4	25.5	1.34
0.29-0.68	2.78	3.58	34.1	11.6	31.9	1.05
0.68-1.22	2.14	2.91	33.3	10.6	34.2	0.91
1.22-1.91	2.12	2.16	23.6	8.6	29.9	0.99
Bottom						
0-0.29	2.99	2.90	34.4	10.5	34.3	1.17
0.29-0.54	2.65	2.92	35.1	10.4	40.1	0.92
0.54-0.72	2.69	2.88	34.2	9.5	35.7	0.91
0.72-0.93	2.16	2.51	32.3	9.1	35.2	0.77
0.93-1.16	2.17	2.49	32.4	10.0	39.0	0.77
GH-78-1						
Top						
0-0.34	1.75	5.03	48.3	17.7	54.8	–
0.34-1.40	0.65	2.26	46.9	13.7	45.7	–
1.40-2.83	0.78	2.19	49.0	12.5	44.8	–
2.83-3.29	1.22	2.34	46.6	14.4	52.8	–
Side						
0-0.16	2.68	5.14	48.3	19.7	60.3	–
0.16-0.32	1.57	4.40	44.5	19.4	57.6	–
0.32-0.50	1.30	3.85	45.3	19.0	57.9	–
0.50-0.73	0.85	3.01	46.9	18.6	55.0	–
0.73-0.98	0.86	2.56	48.3	16.3	55.8	–
Bottom						
0-0.33	5.11	6.97	48.0	29.3	60.2	2.08
0.33-0.53	–	–	–	–	–	–
0.53-0.95	3.95	4.16	49.7	28.5	65.4	1.53
0.95-1.31	4.22	5.18	–	26.4	58.4	1.20
1.31-1.82	2.43	3.43	43.4	21.8	55.0	0.83

depth, while the concentrations of the acid soluble fraction (A) are rather constant (Fig. 5). This may be due to the deposition or adsorption of Cu inside the nodule as fraction (A), which directly comes from diffusing sea water, and the formation of its oxide (fraction B) during the rearrangement of the crystal structure of the ferro-manganese oxide. We conclude from these results that the bottom surface of the equatorial nodules is now growing by making up of substances existing at the sediment-nodule interface. In other words the bottom surface of nodules grows in the region where Mn is remobilized.

Radiochemical evidences on the variety of manganese nodules The analytical data of Th isotopes are given in Table 3. Thorium is known to be one of the elements being most actively removed in the ocean (e.g. TSUNOGAI and MINAGAWA, 1978). The concentration of ^{230}Th (half life, 75,000yr), a daughter of ^{234}U, decreases with depth in the nodules owing to its radioactive decay. The growth rates of nodules, evaluated from the depth gradients of excess ^{230}Th or the ratio of excess ^{230}Th/^{232}Th are listed in Table 4. They are about 2 to 3mm/million years for all the depth intervals studied, which are similar to those of pelagic nodules deter-

mined by various authors (e.g. KRISHNASWAMI and COCHRAN, 1978).

For the subtropical nodule (KH-79-4), the growth rate of the bottom side is not reliable because of the low concentration of ^{230}Th. However, it is similar to those (rates) for other sides where the concentration of ^{230}Th is high. If the top surface of the nodule is allowed to stand for 300,000 years (four half lives of ^{230}Th), the activity ratio of ^{230}Th/^{232}Th will be equal to that of the bottom surface. KRISHNASWAMI and COCHRAN (1978) have observed the same phenomenon and postulated that the nodules accumulate these nuclides only when they are in contact with sea water and that nodules are sometimes turned over on the sediments. MOORE *et al.* (1981), however, have hypothesized, based on the ratio of ^{231}Pa/^{230}Th, that both sides of nodules are growing simultaneously and an interstitial water source contributes to the accretion of Mn and other material on the bottom surface. They found that the ratio of ^{231}Pa/^{230}Th at the bottom surface of nodules was not less than that at the top surface. ^{231}Pa is a daughter of ^{235}U and its half life (32,500 yr) is about one half of that of ^{230}Th. Thus, the concentration of ^{231}Pa decreases more rapidly with time than that of ^{230}Th (e.g. the ratio of ^{231}Pa/^{230}Th decreases by a factor of 5 after 300,000 yr). Since we did not determine ^{231}Pa and the observed ^{231}Pa data in the literature (e.g. MOORE *et al.*, 1981) are not so reliable to calculate the growth rate of the bottom surface because of analytical difficulty, we attempted to solve this problem with a different approach.

The bottom surfaces of the subtropical nodules (KH-79-4) smaller than 5 cm in diameter show ^{230}Th concentration as high as for the top surfaces, in contrast to the low ^{230}Th in the

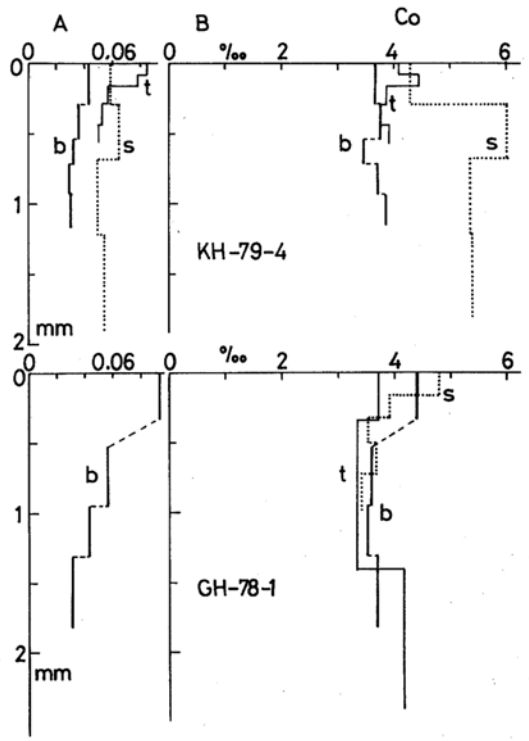

Fig. 4. Depth profiles of the weak acid soluble (A) and the oxide (B) fractions for Co. The symbols are the same as those in Fig. 2.

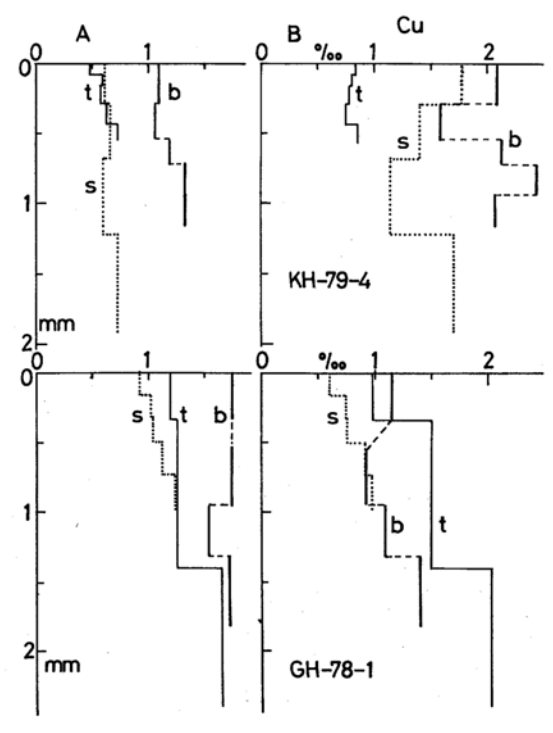

Fig. 5. Depth profiles of the weak acid soluble (A) and the oxide (B) fractions for Cu. The symbols are the same as those in Fig. 2.

Table 3. Concentrations of Th isotopes in nodules.

Depth (mm)	^{230}Th (dpm/g)	^{232}Th (dpm/g)	^{228}Th (dpm/g)
KH-79-4			
Top			
0-0.08	831 ±40	24.1 ±1.6	20.8 ±1.4
0.08-0.16	609 ±34	20.5 ±1.5	17.8 ±1.3
0.16-0.29	430 ±24	20.1 ±1.3	18.9 ±1.3
0.29-0.44	330 ±16	18.2 ±1.0	18.1 ±1.0
0.44-0.57	257 ±15	16.4 ±1.3	18.8 ±1.4
Side			
0-0.29	676 ±38	22.1 ±1.4	19.2 ±1.3
0.29-0.68	110.7 ± 5.4	14.7 ±0.9	14.8 ±0.9
0.68-1.22	22.7 ± 1.5	14.4 ±1.1	15.1 ±1.0
1.22-1.91	10.7 ± 0.7	9.3 ±0.6	11.6 ±0.8
Bottom			
0-0.29	52.5 ± 2.2	10.3 ±0.8	15.9 ±1.0
0.29-0.54	21.5 ± 1.2	12.5 ±0.8	13.3 ±0.9
0.54-0.72	20.4 ± 1.2	9.5 ±0.7	11.1 ±0.8
0.72-0.93	20.0 ± 1.1	10.7 ±0.8	13.0 ±0.9
0.93-1.16	14.1 ± 1.0	8.5 ±0.7	9.0 ±0.7
Interior			
10 (A)	10.94± 0.79	6.62±0.54	7.91±0.61
10 (B)	6.07± 0.45	5.55±0.42	6.52±0.47
30 (C)	3.72± 0.25	2.90±0.21	3.74±0.25
GH-78-1			
Top			
0-0.34	567 ±15	16.3 ±1.3	16.4 ±1.3
0.34-1.40	59.7 ± 2.5	14.3 ±1.1	14.6 ±1.1
1.40-2.83	33.9 ± 1.6	12.0 ±0.9	14.6 ±1.0
2.83-3.29	27.9 ± 1.9	7.6 ±0.8	9.2 ±1.5
Side			
0-0.16	1004 ±46	16.5 ±1.1	17.1 ±1.1
0.16-0.32	394 ±22	12.6 ±1.0	16.8 ±1.2
0.32-0.50	197 ±11	14.6 ±1.2	15.4 ±1.2
0 50-0.73	101.5 ± 5.0	13.6 ±0.9	14.1 ±0.9
0.73-0.98	80.8 ± 4.7	10.8 ±0.8	12.4 ±0.9
Bottom			
0-0.20	531 ±26	11.7 ±0.9	16.6 ±1.1
0.20-0.42	188 ±11	11.8 ±0.9	12.9 ±0.9
0.42-0.72	90.4 ± 5.3	11.0 ±0.8	13.6 ±1.0
0.72-1.18	22.5 ± 1.3	9.4 ±0.7	11.9 ±0.8
1.18-1.78	20.0 ± 1.4	10.3 ±0.8	12.2 ±0.9
Interior			
10(D)	10.38± 0.72	4.73±0.39	6.80±0.51
12 (E)	10.56± 0.77	4.88±0.44	8.39±0.65
17 (F)	8.22± 0.60	5.27±0.43	6.76±0.52
20 (G)	5.50± 0.42	4.13±0.34	5.83±0.44

nodules as mentioned above (Table 5). The larger nodules from the equatorial Pacific (GH-78-1) have high concentration of ^{230}Th and are growing at all surfaces at nearly the same rate. This is confirmed by the results of the three additional nodules collected at the same site (Table 5). We have already stated the bottom surface of the equatorial nodule (GH-78-1) contains more of metastable forms of transition metals. These results may imply that Mn necessary for the growth of manganese nodules is supplied from the oxygenated bottom water where Mn is not truly dissolved, and from pore water in the region where Mn is diagenetically remobilized.

Table 4. Growth rates of nodules based on the excess ^{230}Th and excess ^{230}Th/^{232}Th methods.

	Growth rate* (mm/10^{6}yr) ^{230}Th$_{ex}$	^{230}Th$_{ex}$/^{232}Th
KH-79-4		
Top	2.6	3.5
Side	1.9	2.2
Bottom	(2.0)	(1.8)
GH-78-1		
Top	2.7	2.8
Side	1.8	2.0
Bottom	2.1	2.3

** Values in parentheses are not reliable.*

There is a small systematic difference between the growth rates calculated from excess ^{230}Th alone and those calculated from the ratio of excess ^{230}Th/^{232}Th. This is caused by the decrease in the concentration of ^{232}Th with depth. To make this clearer the concentration of ^{232}Th is plotted against depth in Fig. 6. There is a steep decrease in the concentration of ^{232}Th in the nodule near the surface layer. The bottom surface of the larger subtropical nodule (KH-79-4) contains about half the ^{232}Th compared with other sides or the equatorial nodules (GH-78-1). Although the decrease of ^{232}Th with depth is considered by MOORE *et al.* (1981) to be puzzling, it can be explained if some Th is excluded at the early stage of the diagenetic rearrangement of ferromanganese oxide crystals and if the bottom surface of the subtropical nodule (KH-79-4) containing low ^{232}Th is not growing at present. This explanation is highly acceptable. However, another possibility still remains as discussed below, in that the bottom surface is now being made up of substances containing low ^{232}Th and ^{230}Th.

The accretion rates of elements to the nodules have been calculated by combining the growth rates of nodules and the concentrations of elements in nodules as given in Table 6. Two or

Table 5. Additional data on the radiochemical components in the bottom surface of some other nodules in contact with sediments.

Size*1	Depth (mm)	^{230}Th (dpm/g)	^{232}Th (dpm/g)	^{230}Th/^{232}Th	$(^{230}Th/^{232}Th)_0$*2
KH-79-4					
(1)	0-0.49	23.5± 1.0	5.9±0.4	4.0±0.3	10
L (2)	0-0.45	32.9± 1.5	5.3±0.5	6.2±0.7	15
(3)	0-0.27	38.2± 1.4	5.5±0.4	7.0±0.6	12
(1)	0-0.44	534 ±31	21.2±1.4	25.2±2.2	59
S (2)	0-0.26	542 ±30	16.1±1.1	33.6±3.0	58
(3)	0-0.61	417 ±24	20.5±0.2	20.4±1.8	61
GH-78-1					
(1)	0-0.38	262 ±13	10.9±0.8	24.1±2.2	51
L (2)	0-0.27	844 ±48	18.8±1.5	44.9±4.4	79
(3)	0-0.29	1080 ±49	13.7±1.1	74.2±7.0	135
cf. surface sediment at KH-79-4 site	0-20	88.9± 2.9	3.6±0.2	24.8±1.2	26

**1 L refers to nodules having diameters larger than 5 cm.*

**2 Values at the sediment-water interface calculated by assuming a growth rate of 2×10^{-6} mm/yr for all the nuclides.*

three accretion rates are given for components whose accretion rate changes monotonously with depth. Their difference is also computed. The fluxes of metals to the nodules are smaller by more than one order of magnitude than the fluxes to the bottom sediments, even for Mn (TSUNOGAI *et al.*, 1979, TSUNOGAI and KUSAKABE, 1982).

Table 6 shows that the weak acid soluble fractions of Mn, Fe and Co, and the total concentration of ^{232}Th decrease with depth in nodules. Conversely, the total and oxide fractions of Mn for both sites and Ni and Cu for the equatorial site (GH-78-1) increase with depth in the nodules. The acid soluble fractions of Cu and Ni in the equatorial nodule also increase with depth, although the extent of them is much smaller than that of oxide fractions. These results confirm the conclusion described in the previous section for chemical elements, in that post crystalization process in nodules induces the exchange of metal ions.

The surface values of accretion rates of ^{232}Th are generally proportional to those of Al and Si except for the bottom surface of the subtropical nodule (KH-79-4). However, the trend in the depth profile of ^{232}Th is fairly different from those of Al and Si (Table 6). Furthermore the ratio of ^{232}Th/Al in the nodule

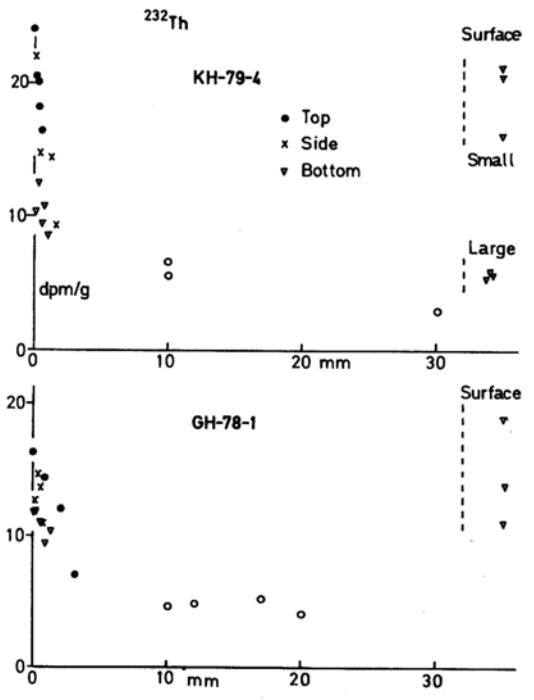

Fig. 6. Variation of the ^{232}Th concentration with depth from the variation surface. Additional data on the ^{232}Th concentration in the bottom surface layer of the other nodules are also shown on the right hand side.

Table 6. Accretion rates of chemical components (in ng/cm²/yr) and Th isotopes (in 10^{-5} dpm/cm²/yr) in the nodules. For components monotonously increasing or decreasing with depth, values at 2 or 3 different depths and their differences are shown.

	Depth (mm)	Mn				Fe				Al				Si
		A	B	C	Σ	A	B	C	Σ	A	B	C	Σ	Σ
KH-79-4														
Top	0	4.44	99	0.52	104	6.10	100	33	137	1.95	3.02	10.8	15.8	35.6
	0.5	4.07	113	0.33	117	4.48	103	26	133	2.24	3.29	12.7	18.2	39.6
	Δ (0-0.5)	−0.37	+13	−0.19	+13	−1.62	+3	−7	−4	+0.29	+0.27	+1.9	+2.4	+4.0
Side	0	2.16	77	0.43	79	2.03	48	27	76	0.80	1.47	6.3	8.6	22.7
	1	1.69				1.64				1.10	2.48	3.9	7.5	19.8
	Δ (0-1)	−0.47	0	0	0	−0.39	0	0	0	+0.30	+1.01	−2.4	−1.1	−2.9
Bottom	0	1.62	53	0.34	54	1.13	38	16	55	1.77	3.28	10.4	15.5	26.7
	1	1.28	58	0.22	59	1.16	45	18	64		3.57	5.9	11.2	19.9
	Δ (0-1)	−0.34	+5	−0.12	+5	+0.03	+7	+2	+9	0	+0.29	−4.5	−4.3	−6.8
GH-78-1														
Top	0	1.75	98	1.50	101	4.09	77	–	–	2.07	2.23	–	–	13.7
	1	1.14	109		111	1.84	80	–	–			–	–	
	Δ (0-1)	−0.61	+11	0	+10	−2.25	+3	–	–	0	0	–	–	0
Side	0	1.88	68	0.72	70	3.51	65	9.3	78	1.24	1.32	2.05	4.6	10.0
	1	0.68	74	0.82	76	1.50	57	8.4	67	1.50	1.61	1.68	4.8	
	Δ (0-1)	−1.24	+6	+0.10	+6	−2.01	−8	−0.9	−11	+0.26	+0.29	−0.37	+0.2	0
Bottom	0	3.91	73	1.55	78	4.69	62.6	5.0	72	2.52	2.52	2.12	6.9	11.1
	1	2.96	79		83	2.82	60.3	5.5	69	2.17				
	1.5	2.14	86		90	2.13	59.8	6.3	68	2.04				11.5
	Δ (0-1)	−0.95	+6	0	+5	−1.87	−2.3	+0.5	−3	−0.35	0	0	0	0
	Δ (1-1.5)	−0.82	+7	0	+7	−0.69	−0.5	+0.8	−1	−0.13	0	0	0	+0.4

	Depth (mm)	Ni A	Ni B	Ni Σ	Cu A	Cu B	Cu Σ	Co A	Co B	Co Σ	^{232}Th Σ	^{230}Th Σ
KH-79-4												
Top	0	0.28	1.75	2.03	0.32	0.56	0.88	0.059	2.81	2.86	1.69	65
	0.5	0.40		2.15	0.51		1.07	0.035			1.15	–
	Δ (0-0.5)	+0.12	0	+0.12	+0.19	0	+0.19	−0.024	0	0	−0.54	–
Side	0	0.31	2.55	2.86	0.27	0.63	0.90	0.027	2.29	2.32	0.97	51
	1							0.023			0.63	–
	Δ (0-1)	0	0	0	0	0	0	−0.004	0	0	−0.34	–
Bottom	0	0.16	1.42	1.62	0.39	0.74	1.13	0.016	1.32	1.33	0.41	3.6
	1		1.54	1.70	0.48		1.22	0.011	1.39	1.40	0.35	–
	Δ (0-1)	0	+0.08	+0.08	+0.09	0	+0.09	−0.005	+0.07	+0.07	−0.06	–
GH-78-1												
Top	0	0.44	2.06	2.50	0.67	0.55	1.22	–	2.09	2.09	0.91	53
	1	0.41	2.59	3.00	0.71	0.84	1.55	–			0.80	–
	Δ (0-1)	−0.03	+0.53	+0.50	+0.04	+0.29	+0.33	–	0	0	−0.11	–
Side	0	0.26	1.05	1.31	0.37	0.24	0.61	–	1.91	1.91	0.66	62
	1	0.30	1.51	1.81	0.49	0.39	0.88	–	1.36	1.36	0.43	–
	Δ (0-1)	+0.04	+0.46	+0.50	+0.12	+0.15	+0.27	–	−0.55	−0.55	−0.23	–
Bottom	0	0.46	1.10	1.56	0.77	0.48	1.25	0.043	2.02	2.06	0.54	36
	1	0.50	1.41	1.91				0.020	1.65	1.67	0.45	–
	1.5		1.78	2.28	0.79	0.64	1.43	0.014				–
	Δ (0-1)	+0.04	+0.31	+0.35	0	0	0	−0.023	−0.37	−0.39	−0.09	–
	Δ (0-1.5)	0	+0.37	+0.37	+0.02	+0.16	+0.18	−0.006	0	0	0	–

surface in contact with sea water (*ca.* 1,000dpm/g) is larger than that of the bottom surface of the subtropical nodule (*ca.* 300dpm/g). This is also much larger than that of the bottom sediment (*ca.* 50dpm/g). These suggest that Th has a dual character in its behavior or origin. One aspect of Th is similar to other insoluble components, Al and Si, but the other aspect is different from those on the deep sea bottom. Table 5 also shows that the activity ratio of $^{230}Th/^{232}Th$ of the surface sediment (26 at the KH-79-4 site) is much smaller than those (60) of the bottom surface of small nodules and of other surfaces of nodules in contact with sea water. This is not caused by the bioturbation of the bottom sediment. These results lead us to conclude that there are at least two sources of the Th isotopes in nodules and bottom sediments. One source has an activity ratio of $^{230}Th/^{232}Th$ less than 26 or near 1 which is the value observed in coastal sediments. This consists probably of aluminosilicate debris which comprizes a major part of the Th in sediments. The other source has an activity ratio greater than 60, this may originate from dissolved components or fine particles in sea water and is a major source of Th in the nodule surface in contact with sea water.

Although the concentration of ^{230}Th at the bottom surface of the subtropical nodule (KH-79-4) is less by a factor of 10 to 20 than those at the other surfaces, its ratio of $^{230}Th/Al$ (2,300 dpm/g) is still greater than that of the surface sediment (1,300dpm/g). Therefore, if the sedimentary source of Th (aluminosilicate debris) has small $^{230}Th/^{232}Th$ ratio like that in the coastal sediments, the following possibility arises; The bottom surface of the subtropical nodule (KH-79-4) is also growing at present without turnover and without supply of metals from pore water. The pore water contains no appreciable amount of Mn in the red clay sedi-

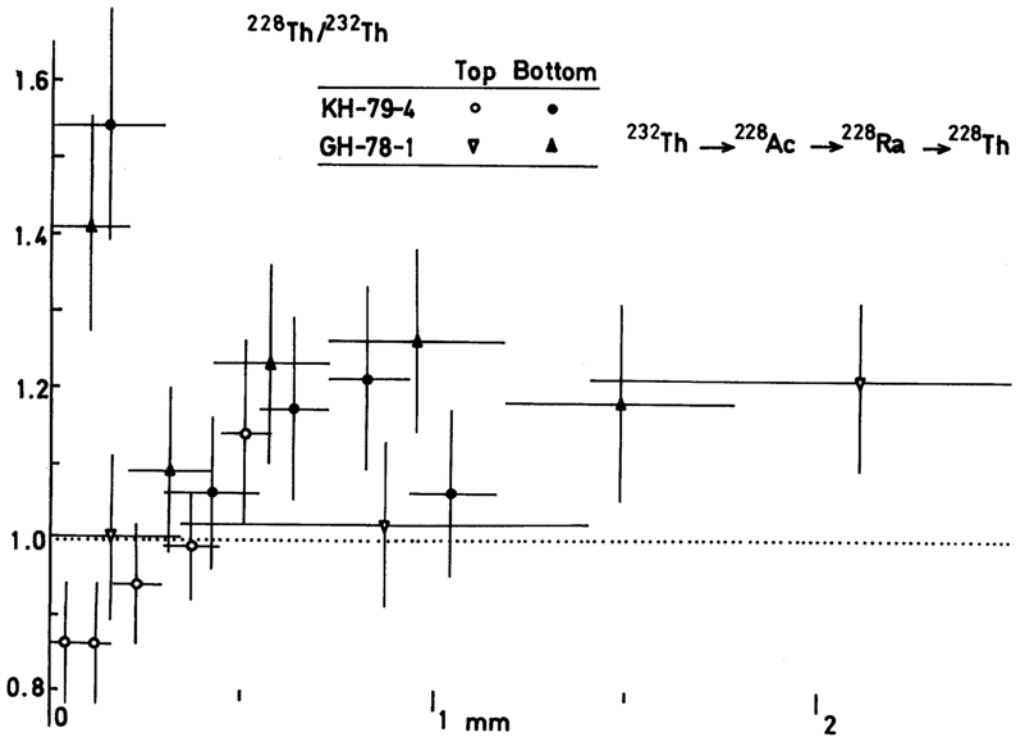

Fig. 7. Depth profiles of ratios of $^{228}Th/^{232}Th$. Open circles and triangles refer to those ratios in the top surface samples as explained in the figure.

ment (TSUNOGAI and KUSAKABE, 1982). It is interesting to note that the bottom surface of the subtropical nodule contains much total Al and Si, because this implies a larger contribution of the former source of Th having a small $^{230}Th/^{232}Th$ ratio. Our data, however, are not sufficient to draw a rigorous conclusion about the validity of this hypothesis.

The activity ratio of $^{228}Th/^{232}Th$ shows a distinctive vertical profile (Fig. 7). The nuclide, ^{228}Th (half life, 1.9 yr), is one of daughters of long-lived ^{232}Th and the secular radioactive equilibrium between ^{232}Th and ^{228}Th is expected if ^{228}Th and its precursors, ^{228}Ra (half life, 5.75 yr) and ^{228}Ac, do not migrate in the nodules. For both the subtropical (KH-79-4) and equatorial (GH-78-1) nodules the activity ratios are larger at the bottom surface wich is in contact with sediments. However, the ratios are less than one at the top surface which is exposed to sea water. The ratios are somewhat larger than unity in the layer at 0.5 to 1.0 mm depth. Similar results have been obtained by KRISHNASWAMI and COCHRAN (1978) for ^{228}Th and by MOORE *et al.* (1981) for ^{226}Ra. This may be due to the migration and deposition of ^{228}Th's precursor ^{228}Ra and/or ^{228}Th itself in nodules and sediments owing to the recoil energy of newly produced hot atoms.

Minerals identified by the X-ray diffraction analysis The manganese nodules consist mostly of amorphous manganese oxides. The identification of their crystal forms from their weak diffraction spectra, however, is rather difficult. Table 7 shows the mineral identification from the X-ray diffraction analysis. Clay minerals or quartz, however, give sharp diffraction peaks in some samples. Thus we have classified the samples into three groups according to the X-ray diffraction patterns. They are the surface layer of the equatorial (GH-78-1) nodule, the surface layer of the subtropical (KH-79-4) nodule and the interior of both nodules. There was no difference between the top and bottom surfaces of either nodule. The surfaces of the equatorial nodule show no quartz peak. This coincides with the low concentrations of major components, Si and Al, of continental debris in the equatorial nodule (Table 1). There is no distinct difference in the absorption spectra between the top and bottom sides for both the nodules. This implies that the diagenetic rearrangement process of crystals causes the spectral difference to occur in the interior of nodules at its later stage of development. It could also imply that the variability in the concentrations of metastable chemical species in the outer few mm layer is due to a small difference in the amount of amorphous or weakly crystalized Mn oxide which comprises a major part of all the nodule samples.

Table 7. Minerals assigned by X-ray diffraction.

Sample	KH-79-4	GH-78-1
Top surface	Todorokite and/or δ MnO_2 and/or Birnessite	Todorokite (no Quartz)
Bottom surface	Todorokite and/or δ MnO_2 and/or Birnessite	Todorokite (no Quartz)
Interior	δ MnO_2 or Birnessite	δ MnO_2 or Birnessite

Acknowledgement—We are grateful to Dr. T. MORITANI and Prof. N. TAGA for their help in the sampling during the Hakurei Maru GH-78-1 and Hakuho Maru KH-79-4 cruises, respectively. We wish to express our appreciation also to Prof. T.-L. KU for valuable comments and to Dr. H. MARING for reading the manuscript. Thanks are due to our many colleagues for stimulating and helpful discussion. Finally we are much indebted to Dr. N. TAKEMATSU for the identification of minerals.

REFERENCES

BURNS, R. G. (1976) The uptake of cobalt into ferromanganese nodules, solids and synthetic manganese (IV) oxides. *Geochim. Cosmochim. Acta* **40**, 95–102.

CRONAN, D. S. (1976) Manganese nodules and other ferro-manganese oxide deposits. *Chemical Oceanography* 2nd ed. Vol. 5, p217–263, ed. by J. P. RILEY and R. CHESTER, Academic Press, London.

HARADA, K. (1977) Marine manganese nodules. *Kaiyo Kagaku*, **9**, 410–429, 480–490, 635–645.

KRISHNASWAMI, S. and COCHRAN, J. K. (1978) Uranium and thorium series nuclides in oriented fer-

romanganese nodules: growth rates, turnover times, and nuclide behavior. *Earth Planet. Sci. Lett.* **40**, 45–62.

KU, T.-L. and BROECKER, W. S. (1969) Radiochemical studies on manganese nodules of deep-sea origin. *Deep-Sea Res.* **16**, 625–637.

MOORE, W. S., KU, T.-L., MACDOUGALL, J. D., BURNS, V. M., BURNS, R., DYMOND, J., LYLE, M. W. and PIPER, D. Z. (1981) Fluxes of metals to a manganese nodule: Radiochemical, chemical, structural and mineralogical studies. *Earth Planet. Sci. Lett.* **52**, 151–171.

NORIKI, S., NAKANISHI, K., FUKAWA, T., UEMATSU, M., UCHIDA, T. and TSUNOGAI, S. (1980) Use of a sealed teflon vessel or the determination of chemical constituents of various marine samples. *Bull. Faculty Fish. Hokkaido Univ.* **31**, 354–361.

TAKEMATSU, N. (1979) The incorporation of minor transition metals into marine manganese nodules. *J. Oceanogr. Soc. Japan* **35**, 191–198.

TSUNOGAI, S. and KUSAKABE, M. (1982) Migration of manganese in the deep sea sediments. *The dynamic environment of the ocean floor,* ed. by K. A. FANNING and F. T. MANHEIM, 257–273.

TSUNOGAI, S. and MINAGAWA, M. (1978) Settling model for the removal of insoluble chemical elements in seawater. *Geochem. J.* **12**, 81–88.

TSUNOGAI, S., YONEMARU, I. and KUSAKABE, M. (1979) Post depositional migration of Cu, Zn, Ni, Co, Pb and Ba in deep sea sediments. *Geochem. J.* **13**, 239–252.